

# A RISK-BASED EVALUATION OF DIRECT DISPLACEMENT-BASED DESIGN

Luke van der Burg<sup>1</sup>, Mohsen Kohrangi<sup>2</sup>, Dimitrios Vamvatsikos<sup>3</sup>, Paolo Bazzurro<sup>4</sup>,

<sup>1</sup>University School for Advanced Studies IUSS Pavia, Italy. (currently Holmes Consulting LP, New Zealand)

<sup>2</sup>RED Risk Engineering + Development, Pavia, Italy

<sup>3</sup>Associate Professor, School of Civil Engineering, National Technical University of Athens, Greece

<sup>4</sup>Professor, University School for Advanced Studies IUSS Pavia, Pavia, Italy

## ABSTRACT

Recent seismic design approaches developed under the umbrella of performance-based earthquake engineering (PBEE) pursue pre-defined performance objectives in terms of structural response, economic losses, or casualties. The earlier PBEE methods were mainly concerned with the deterministic evaluation of performance at a single ground motion intensity level. This premise, however, provides little insight into the long-term risk-based performance of a structure, and limits the ability to make informed design decisions. Given the inherent sources of uncertainty in all aspects of seismic design, probability theory needs to be employed to enable reliable design solutions. However, applying a risk-oriented design approach is not currently feasible for most practitioners, making it essential to understand how the current deterministic applications of these intensity-based PBEE approaches perform in terms of risk. Specifically, the aim is to investigate the capability of the *direct displacement-based design* (DDBD) method in producing reliable, risk-consistent designs. A probabilistic PBEE assessment framework is applied as the benchmark to determine the risk of exceeding performance objectives for multiple DDBD-based reinforced-concrete-wall and dual reinforced-concrete-wall/steel-frame buildings located at three different sites. The significant variation in the achieved risk estimates related to the limit states of damage limitation, life safety and global collapse for the buildings considered, questions the ability of DDBD—or any other intensity-based design method that does not account for uncertainty—to offer risk consistency.

## KEYWORDS:

Direct displacement-based design; Seismic risk; Performance-based earthquake engineering; Seismic hazard.

## INTRODUCTION

The state-of-the-art in performance-based earthquake engineering (PBEE) (Cornell and Krawinkler 2000; Deierlein et al. 2003; FEMA 2018) provides the necessary probabilistic tools for a risk-consistent seismic assessment of existing buildings, accounting for many sources of uncertainty and for as many *performance measures* as desired. Such measures can be defined in terms of *engineering demand parameters* (EDPs), such as the peak inter-storey drift or the peak floor acceleration, or through more informative parameters in terms of *decision variables*, such as economic and human losses or downtime. This naturally leads to the assessment of the mean annual rate (MAR) of exceeding any performance measure threshold of interest. This paradigm can be employed for the design of new buildings (or the rehabilitation of existing ones) by pairing specific performance measure thresholds characterizing, e.g., damage limitation (DL), life safety (LS), or global collapse (GC), with a maximum allowable MAR of exceeding them (Vamvatsikos et al. 2020) to define *performance objectives* for the design. While this is an appealing (and scientifically applicable) proposal for reliable seismic design, the computational burden and the advanced knowledge required either puts performance-based seismic design (PBSD) out of reach for many practitioners, or it is simply not

warranted for most projects. Even though in recent years several novel design methodologies were proposed by researchers to facilitate the implementation of the state-of-the-art in PBSD (Wen 2001; Krawinkler et al. 2006; Franchin and Pinto 2012; Zareian and Krawinkler 2012; Vamvatsikos et al. 2016; Vamvatsikos and Aschheim 2016; Franchin et al. 2018; Žižmond and Dolšek 2019; O'Reilly and Calvi 2019, 2020; Shahnazaryan and O'Reilly 2021), the traditional intensity-based approaches are still dominating design applications.

There is a fundamental difference between having an intensity versus a risk basis (Vamvatsikos 2017). Consider a performance objective pairing an inter-storey drift threshold of 2% with a maximum allowable probability of exceedance (PoE) of 10% in 50 years, henceforth designated as 10/50, which is equivalent to a MAR of  $-\ln(1 - 0.1)/50 \approx 0.0021 \text{ years}^{-1}$ . A risk-based procedure would require checking at the level of the performance measure, here the inter-storey drift, by assessing the PoE of exceeding the threshold of 2% to ensure that it is less than or equal to 10/50. This would require obtaining structural analysis results at multiple intensity measure (IM) levels, assessing the conditional PoE at each and integrating with the frequency of each IM occurring (Cornell et al. 2002). Instead, an intensity-based approach would be satisfied by checking at a single IM level only, verifying that the inter-storey drift assessed at the intensity level with an exceedance frequency of 10/50 does not surpass the 2% threshold. Clearly, these two checks are not the same, and the intensity-based one is by far the simpler. How well it measures up to the risk-based result is not obvious and understanding the factors that come into this requires delving into the details of each intensity-based approach.

The Force-Based Design (FBD) philosophy is by far the most prevalent intensity-based approach, adopted by design codes such as EC8/EN1998-1 (CEN 2004a), NZS 1170.5 (NZS 2004) and ASCE 7-16 (ASCE/SEI 2017). In most of its incarnations it relies on a single intensity level that is typically tied to an LS performance objective, which it tries to satisfy through providing sufficient strength and strict detailing in the critical elements. This process is performed using a single design spectrum, in most cases approximately corresponding with the Uniform Hazard Spectrum (UHS) with a 10/50 PoE. Additional performance objectives, e.g., related to GC or DL may also be satisfied, either explicitly, via a stiffness or deformation check for DL, or implicitly, by ensuring adequate ductility capacity to delay the appearance of GC. Still, even when explicitly verified, such checks tend to be tied to the same 10/50 design intensity level. As linear elastic structural models are universally used, the effects of non-linearity, overstrength, and ductility need to be accounted for. This is the premise of the behaviour/response-modification/strength-reduction factor, represented by  $q$  in European codes and  $R$  in USA codes. It typically varies with the type of lateral-load-resisting system, but not the site, and it is used to scale down the design spectrum to account for the beneficial effects of a stable, non-linear behaviour. Structural members are then sized to limit deformations and sustain the forces and moments developed under the design lateral loads.

FBD has drawn considerable criticism, e.g., by Priestley (1993), due to limitations such as the potential displacement incompatibility with the assumed ductility demand used to justify designing for forces less than the elastic force level. To address such limitations the concept of Displacement-Based Design (DBD) was proposed (e.g. Moehle 1992; Priestley et al. 2007). Direct displacement-based design (DDBD) is currently the most developed DBD method with a recent update to the subject text and a model seismic code (Sullivan et al. 2012). The fundamental philosophy behind DDBD is to design structures by proportioning strength and stiffness to achieve—rather than be bounded by—a given performance objective under a specified level of seismic intensity (Priestley et al. 2007). This is in contrast to FBD, where the satisfaction of the performance objective is checked at the end of the design process. Further differences include the use of a 10/50 displacement (rather than acceleration) design spectrum, while in place of a  $q$  or  $R$  factor, the design spectrum is reduced as a function of the expected ductility demand compatible with the displacement-based design objectives.

As DDBD aims directly to attain a given performance, one may believe that the method produces structures with the desired risk of the performance objective not being met, irrespective of the seismicity characteristics at the site (see chapter 3 of Priestley et al. 2007). This expectation inherently relies on the assumption that a deterministic intensity-based check is equivalent to a probabilistic risk-based one (Bazzurro et al. 1998). Such a belief trusts, rather naively, that a simplified pseudo-static method that is incapable of dealing with the complexities of the building's dynamic behaviour under the excitation of real ground motions is unaffected by uncertainties in the expected ground motion characteristics and in the structural capacity. This reasoning is faulty. Overall, the intensity-basis employed by FBD, DBD, and DDBD is prone to non-conservativeness by neglecting uncertainties. Mitigating this inconsistency without resorting to explicit PBSD is not easy. Codes typically make up for the shortfall by employing conservative assumptions and by enforcing design minima, attempting to tune the risk across broad classes of lateral-load-resisting

systems in an effort that often (yet not always) ends up decreasing the risk well below the requirements of the performance objective (Iervolino et al. 2018). Still, this cannot guarantee designs with a *target uniform risk* for any limit-state in the non-linear range of response across different sites and structural systems. More nuanced site and system specific approaches are thus required. This is the premise of risk-targeted design spectra (Luco et al. 2007) and risk-consistent  $R$  or  $q$  factors.

Risk-targeted spectra adjust the main design input of the seismic load to achieve a single performance objective defined at the level of a generic fragility curve representation of actual structures. As adopted in ASCE 7-16, they target a collapse PoE of 1/50 (a risk basis) assuming that the system has a collapse probability of 10% at an intensity level of 2/50 (an intensity basis). In broad terms, risk targeted spectra can be said to offer a link between the desired risk-basis and the actually employed intensity-basis, attempting to ensure that verifying the latter will result in the desired performance, at least in an average sense across buildings of different classes located at different sites (see Gkimpraxis et al. (2019) and Spillatura et al. 2022). To also ensure this performance irrespective of the structural system, risk-targeted spectra need to be employed in tandem with properly calibrated  $q$  or  $R$  factors to ensure that a system designed by the code will conform to the adopted generic fragility curve representation, e.g., by having a collapse probability of 10% at an intensity level of 2/50 (FEMA 2009). Obviously, such broad generalizations and large-scale calibrations take their toll. Thus, risk-targeted spectra cannot guarantee the performance of any specific structure; however, in respect to the single targeted performance objective (e.g., collapse) they move towards producing harmonised (i.e., more uniform) risk across buildings at different sites (Spillatura et al. 2019). Extending to multiple pre-defined objectives and achieving higher fidelity requires a more fine-grained calibration of both aspects of this process, with a better characterization of lateral-load-resisting systems than a generic fragility curve, as well as the employment of risk-consistent  $q$  or  $R$  factors to accurately capture performance (Vamvatsikos et al. 2020). Clearly, this is a FBD-compatible process, but it also shows a potential path for improving all other intensity-based approaches, tuning similar knobs of DBD and DDBD to better harmonize the resulting risk.

With the continued advances in computer tools and recognition of the applicability of probabilistic methods by engineers, it is likely that risk-based PBSB will eventually form the future generations of seismic design; however, there still seems to be a long way to achieving this goal. Until then, the current design approaches need to be validated and possibly adjusted to ensure that our structural design outputs are risk-consistent while maintaining the required simplicity necessary for common practice. At the very least, if we adopt simplified alternatives, we should be aware of the penalties associated with the shortcut to success. Following this path, we aim to quantify the risk-oriented capabilities of the DDBD method.

## **DDBD VERSUS THE STATE-OF-THE-ART IN PBEE**

FBD characterises the structure in terms of the elastic, pre-yield properties; DDBD instead uses the secant stiffness,  $K_e$ , at the maximum design displacement,  $\Delta_d$ , that achieves the performance objective. In lieu of the arbitrary ductility allocation, in the form of a  $q$  or  $R$  factor assigned to the system as a whole and without consideration of displacement compatibility, DDBD accounts for energy dissipation with the assignment of equivalent viscous damping,  $\zeta$ , at a level representative of the combined elastic damping and the hysteretic energy absorbed during the inelastic response. For multi-degree-of-freedom (MDOF) buildings, the method relies on the substitute structure approach (Shibata and Sozen 1976) in which the equivalent mass,  $m_e$ , the design displacement,  $\Delta_d$ , and the corresponding effective damping,  $\zeta_e$ , estimated from the expected ductility demand, are determined in terms of an equivalent single degree of freedom (SDOF) system. This step requires an assumed non-linear displaced shape of the structural system at the design level that produces the limit state threshold value of displacement or drift for the most critical member (Figure 1a). The effective period,  $T_e$ , of the equivalent SDOF system is then read from the damped displacement spectrum at the point corresponding to the design displacement measured at the effective height,  $H_e$  (Figure 1b). Once the characteristics of the substitute structure are determined, the design base shear is calculated (Figure 1c) and distributed to the discretised mass locations up the height of the MDOF model in proportion to the mass and design inelastic displacement, not unlike what is done in force-based design. Thus, the process determines the strength required at designated plastic hinge locations to achieve the displacement-based objectives, which is then combined with capacity design procedures calibrated to the DDBD method such that non-ductile modes of inelastic deformations are prevented.

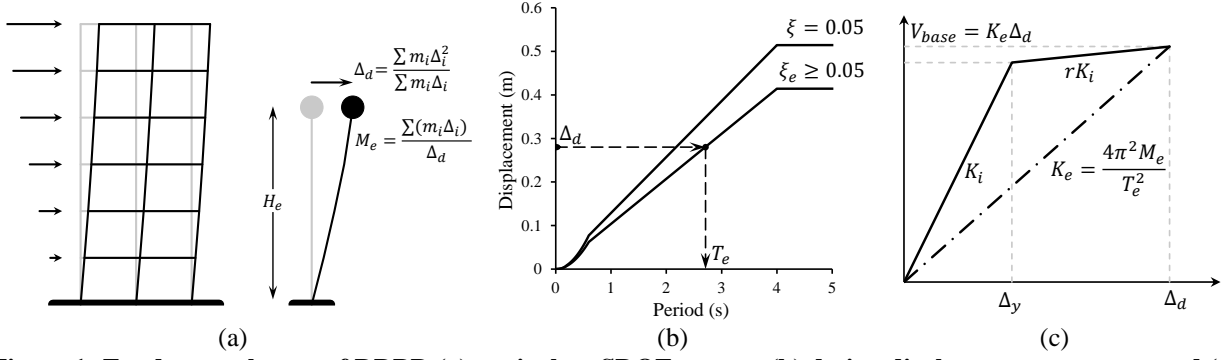


**Figure 1: Fundamental steps of DDBD (a) equivalent SDOF system, (b) design displacement spectrum and (c) effective stiffness representation**

In comparison, the state-of-the-art PBEE framework adopted by the PEER Center (Cornell and Krawinkler 2000) estimates the highly complex relationship that maps the ground motion input to the non-linear response output with a detailed analysis of the dynamic behaviour induced by hazard consistent ground motions at many intensity levels. Moreover, the probabilistic framework allows for the incorporation and propagation of sources of uncertainty associated with the inherent randomness of nature and uncertainties associated with the lack of knowledge about the phenomena being modelled. This procedure is a conceptual method that estimates the annual frequency of exceedance,  $\lambda(DV)$ , of one or multiple decision variables ( $DV$ ), such as economic losses, downtime, or human casualties, summarised as:

$$\lambda(DV) = \iiint G(DV|DM) \cdot |dG(DM|EDP)| \cdot |dG(EDP|IM)| \cdot |d\lambda(IM)| \quad (1)$$

$G(\cdot)$  is the complementary cumulative distribution function of its argument, while  $\lambda(\cdot)$  is the mean annual frequency of exceeding it.  $DM$  stands for a damage measure showing progressive damage of the structural or non-structural elements and building contents, as a function of several engineering demand parameters ( $EDP$ ), such as storey drift or floor acceleration. Lastly, the  $IM$  is the intensity measure used to define the severity of a ground motion, such as the 5%-damped first-mode spectral acceleration,  $Sa(T_1)$ .

By reducing the order of integration in Equation (1), one can similarly compute  $\lambda(DM)$  or  $\lambda(EDP)$  representing the annual frequency of exceedance of a given damage state or a structural response level, respectively. Through an iterative process, the trial design is thus verified to meet the performance objectives when the MAR of exceeding the respective thresholds in terms of  $DV$ ,  $DM$  or  $EDP$ , i.e.,  $\lambda(DV)$ ,  $\lambda(DM)$  or  $\lambda(EDP)$  are lower than the corresponding targets. As can be implied from Equation (1), there are many practical technicalities engaged in this process, even for the simplest form of evaluating  $\lambda(EDP)$  also dealt with in this study. As such, different aspects of this process have been the subject of a vast amount of research in the past three decades. These mainly include probabilistic seismic hazard analysis (PSHA) (Cornell 1968); the choice of a suitable  $IM$  used as an interface between seismic hazard and structural response (e.g., see (Luco and Cornell 2007; Kohrangi et al. 2016b)); and hazard consistent ground motion record selection to link the seismic hazard at the site to the structural response of interest (such as conditional spectrum (Lin et al. 2013a)). Finally, there is the structural modelling and evaluation of the dynamic response of the building at many  $IM$  levels through different techniques such as incremental dynamic analysis (IDA) (Vamvatsikos and Cornell 2002) or multiple stripe analysis (MSA) (Jalayer 2003), while also accounting for the structural response and modelling uncertainties (Cornell et al. 2002; Porter et al. 2002). In this study, we apply the latest and most recent tools in the field developed to evaluate the  $\lambda(EDP)$  of the case study buildings. This provides an unbiased benchmark to evaluate the capability of the DDBD method to produce buildings with a uniform risk of exceeding the target performance objectives.

## CASE STUDY BUILDINGS AND SITES

We consider two sets of ordinary office buildings (importance class II, according to EC8), covering two different lateral-load-resisting systems. Each set contains three buildings derived from a consistent base model inspired by Garcia et al. (2010), at 4, 7 and 9 stories high—producing six unique building models. The plan geometry of all six building variants is identical with  $5 \times 3$  bays with a bay length of 8.0 metres in both directions. The lateral-load-resisting system of the first set, illustrated in Figure 2a and Figure 2c, is provided by two pairs of identical reinforced concrete (RC) cantilever walls in the transverse direction and steel moment frames in the longitudinal direction. It is assumed that the distance between the two walls at each end of the building is large enough that slab-coupling effects are negligible. The second building set, shown in Figure 2b and Figure 2d, converts the gravity-only steel frames of the first set into steel moment-resisting frames (MRFs), producing steel-frame/RC-wall dual systems. The buildings' layout is regular both in plan and in elevation, and thus simple 2D models may be employed. Herein, only the transverse direction is analysed, as indicated in Figure 3, with the longitudinal direction presented here for completeness. The seismic mass at each level is 1080 tonnes, which includes an allowance for seismic live load and superimposed dead loads of a typical office building.

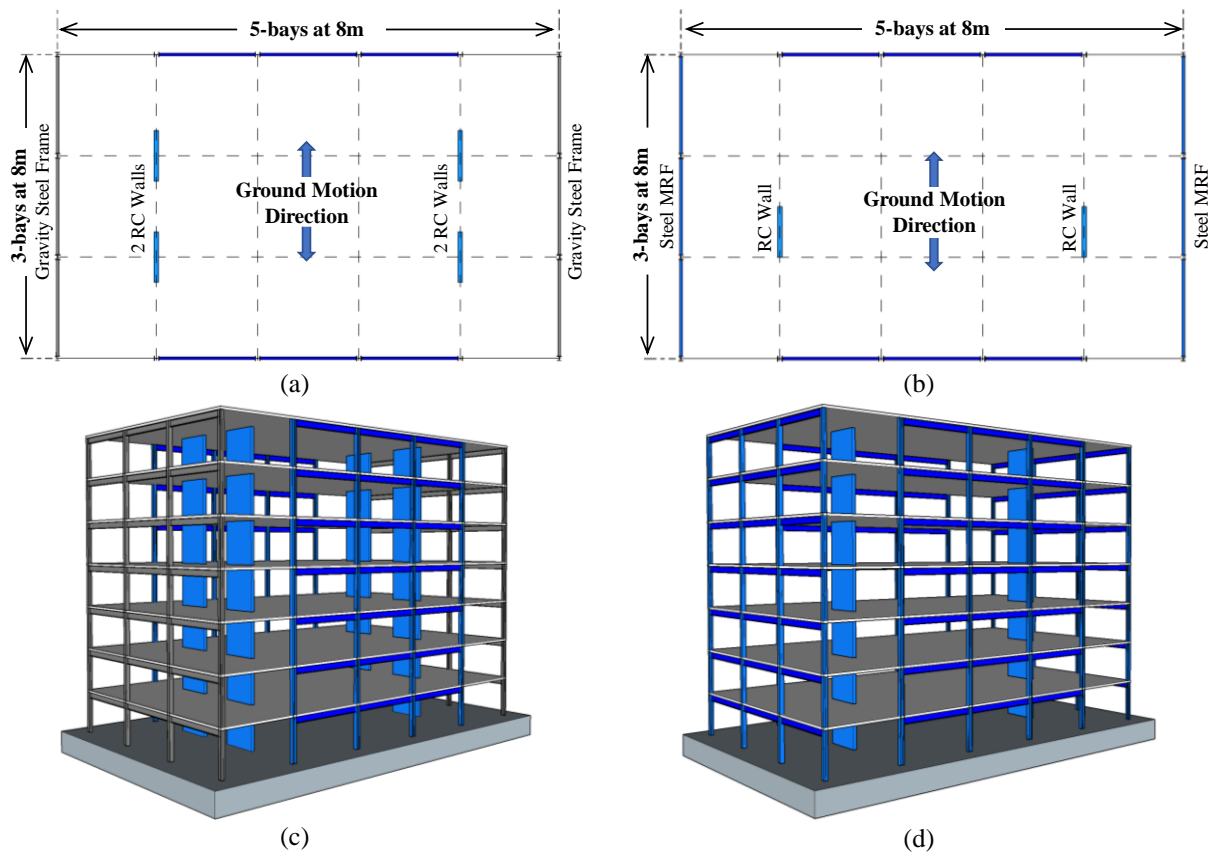


**Figure 2: Illustration of the building configuration showing the plan layout and 3D view of the 7-storey case study buildings for wall systems (a & c) and dual wall-frame systems (b & d). Lateral-load-resisting systems are highlighted in blue. The “ground motion direction” arrows indicate the principal axis analysed in 2D.**

Following the approach by Kohrangi et al. (2017b), three high seismicity sites in Athens ( $37.976^\circ\text{N}$ ,  $23.751^\circ\text{E}$ ), Perugia ( $43.111^\circ\text{N}$ ,  $12.389^\circ\text{E}$ ) and Focsani ( $45.696^\circ\text{N}$ ,  $27.179^\circ\text{E}$ ) are selected to anchor the case study buildings as they share a common reference peak ground acceleration (PGA) on bedrock of  $a_g=0.3g$  at the 10/50 design intensity level as estimated via the ESHM13 seismic source model (Giardini et al. 2014). The Type 1 design spectrum recommended by EC8 for regions of high-seismicity is rigidly anchored to this common reference PGA value. Therefore, provided the soil class is consistent for all sites, the resulting design spectrum is identical, and hence buildings designed for one site are equally suitable for any of the three locations considered (according to the code). Here we assume that all sites are located on soil with averaged shear wave velocity in the top 30 metres of  $V_{S30} = 360$

ms<sup>-1</sup>, corresponding with the borderline of soil type C according to the EC8 soil type classification. In recognition of the fact that the corner period of the design spectrum is a function of the earthquake magnitude and that the cut-off corner period of 2.0 seconds given by EC8 is non-conservative in computing the displacement response spectra (Faccioli et al. 2004; Priestley et al. 2007), the constant velocity region of the response spectrum is continued into the constant displacement region until the corner period of 4.0 seconds. Beyond 4.0 seconds, the spectral displacement is assumed to remain constant.

The buildings are designed to the current Eurocode provisions (CEN 2004a, b, 2005) with DDBD substituted for the code-adopted equivalent lateral force method. Since the former employs set drift thresholds to determine element demands, rather than the combined drift and base shear requirements of FBD, a middle ground is sought to achieve Eurocode compatibility. Specifically, the life-safety (LS) limit state is targeted by imposing an inter-storey drift limit of 2.0% at the 10/50 design ground motion intensity, corresponding to a return period of 475 years. The reason for this choice stems from the damage limitation (DL) requirement of EC8, limiting the inter-storey drift to 1.0% at the 10/10 intensity level for buildings that contain non-structural elements fixed in such a way that they do not interfere with the structural deformations. For importance class II buildings, the code essentially approximates the 10/10 intensity by one-half of the corresponding 10/50 design value, thus, within EC8 a 1.0% drift requirement at 10/10 is equivalent to a 2.0% limit at 10/50. Note that the 50% reduction per EC8 is a reasonable approximation for the three sites considered, resulting to a reduced PGA of 0.173g (soil type C), compared to the site-specific 10/10 PGAs of 0.159g, 0.164g and 0.184g for Athens, Perugia and Focsani, respectively (Giardini et al. 2014). Since the aforementioned translation of the drift limit (twice the intensity causes twice the drift) is based on the equal displacement rule, rather than the equivalent linear SDOF approach of DDBD, one could question whether this 2% drift limit check at 10/50 is equivalent to a 1% drift limit check at 10/10. In fact, with the exception of the 4-storey wall building (at all three locations), when designing to exclusively target the LS performance objective stated above, all buildings also satisfy a drift limit of 1% at the 10/10 intensity level. Or equivalently, according to the DDBD process, these 15 (out of 18 total) buildings achieve the 1% inter-storey drift limit at an intensity more severe than required by EC8. Thus, we may argue that verifying compliance of the final designs to a DL criteria of 1% drift at 10/10 intensity is legitimate for these buildings.

The characteristics of the building designs produced with the DDBD method are summarised in Table 1 (see van der Burg L. (2019) for more details). The structural walls are detailed in accordance with the ductility class high (DCH) provisions of EC8, with the reinforcement reduced along the height of the building in proportion to the decreasing seismic demand.

**Table 1: Summary of building designs based on the DDBD approach for the six case study buildings**

Design Item	Wall Buildings			Dual wall-frame Buildings		
	4-storey	7-storey	9-storey	4-storey	7-storey	9-storey
Wall length and thickness (m × m)	4.0×0.3	5.0×0.3	6.0×0.3	4.0×0.3	5.0×0.3	6.0×0.3
Max reinforcement ratio (%)	1.16	1.92	1.82	1.82	2.09	1.71
Main Beams		—		W21×55	W21×55	W21×62
Roof beams		—		W18×35	W16×36	W18×35
External columns		—		W14×61	W14×61	W14×68
Internal columns		—		W14×120	W14×120	W14×132
Effective period, $T_e$ (s)	2.22	2.95	3.48	1.93	3.10	3.86
Design ductility, $\mu_{sys}$	2.46	1.56	1.41	1.52	1.31	1.27
Base shear coefficient	0.13	0.10	0.09	0.17	0.11	0.09

## STRUCTURAL MODELLING

A 2D fibre-based finite element model (Figure 3) is adopted for all structures, accounting for both stiffness and strength deterioration due to concrete cracking, section yielding, and cyclic loading. The buildings are modelled using SeismoStruct (SeismoSoft 2018), with inelastic frame elements for both the RC and structural steel elements. A force-based lumped-plasticity fibre-section formulation is used for the structural steel elements, while the RC walls are subdivided into one metre segments and modelled with displacement-based distributed plasticity elements. The

Mander et al. (1988) model is assumed for concrete fibres, while the Menegotto-Pinto model (Menegotto and Pinto 1973) is employed for both structural and reinforcement steel. It could be argued that a lumped-plasticity phenomenological model (e.g. Lignos and Krawinkler 2011) would provide higher fidelity for the SMF elements close to collapse, but as the response of the dual systems is dominated by the RC walls (Figure 4), the SMFs are mainly delegated to providing additional stiffness, with their post-yield behaviour being of little consequence. The seismic masses are considered lumped at the floor levels, while diaphragm constraints are enforced at each floor. Full base fixity is assumed. A leaning column is added to carry loads not tributary to the modelled frame, while P- $\Delta$  effects are accounted for via a first-order treatment.

The initial-stiffness Rayleigh damping model is adopted, assuming an equivalent viscous damping coefficient of 1% anchored at the first and second modal periods of each building. This low level of damping is typical for fibre-based models of RC structures (Sousa et al. 2020), as the latter incorporate significant hysteretic energy dissipation from the early stages of nominal “elastic” response due to cracking. The same holds for the dual RC-wall/steel-frame systems, which are dominated by the RC wall response early on, as shown by the pushover analysis in Figure 4 for four-storey dual system. At higher levels of response, hysteretic damping takes over, rendering the initial damping assumption less relevant. The modal vibration periods and modal mass participation factors for the first and second modes of the case study buildings are presented in Table 2.

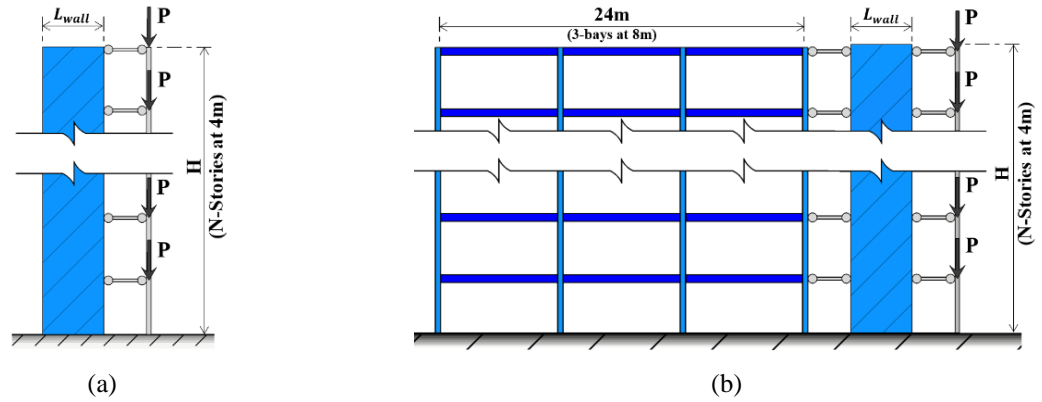


**Figure 3: Schematic illustration of the structural models for: (a) wall system; and (b) Dual wall-frame system. On the right of the RC wall, the leaning column is shown.**

**Table 2: Dynamic characteristics of case study buildings**

No. Stories	Building	Modal period (s)		Mass participation (%)		$\theta_{col}$ (%)
		1 <sup>st</sup> Mode	2 <sup>nd</sup> Mode	1 <sup>st</sup> Mode	2 <sup>nd</sup> Mode	
4	Wall	0.66	0.10	69.5	21.0	4.5
	Dual wall-frame	0.79	0.14	70.2	20.3	4.3
7	Wall	1.28	0.21	65.7	20.2	4.3
	Dual wall-frame	1.53	0.28	66.5	19.3	3.8
9	Wall	1.56	0.25	64.6	19.8	3.9
	Dual wall-frame	1.83	0.34	65.7	18.8	3.4

A non-linear static procedure is used to perform a preliminary structural assessment of the building designs to verify the base shear capacity and to estimate the GC capacity in terms of a maximum inter-storey drift ratio (MIDR) limit,  $\theta_{col}$ . The pushover analysis is performed to a target displacement sufficiently large to estimate the ultimate displacement capacity using an imposed load pattern consistent with the assumed inelastic first mode shape adopted by the DDBD procedure. GC is assumed to occur if either the dynamic analysis algorithm fails to converge due to numerical instability at high deformation levels, or if the MIDR exceeds the pre-defined collapse capacity threshold,

$\theta_{col}$ . More specifically, we assume that  $\theta_{col}$  corresponds with the lowest MIDR value at which: (i) a sudden reduction of at least 40% of the building's total strength occurs, or (ii) the concrete core is crushed at the wall toe and buckling of the flexural reinforcement occurs, as shown in Figure 4. The last column in Table 2 presents the  $\theta_{col}$  values for each building obtained using the above-described method, with a range of 3.4–4.5%.

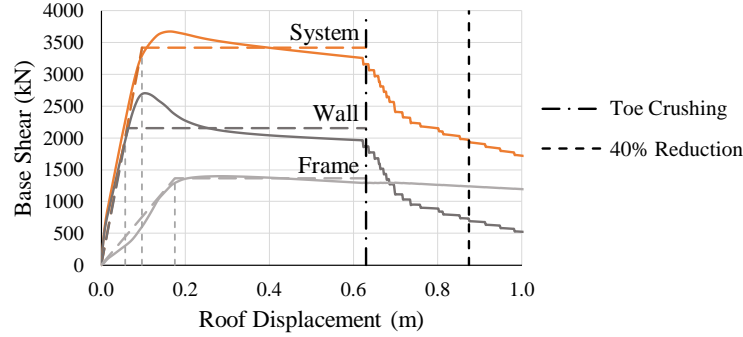


**Figure 4: Pushover curve for the four-storey dual wall-frame system. Toe crushing is the dominant failure mode.**

## IM CHOICE, HAZARD ANALYSIS AND GROUND MOTION DATABASE

A typical choice for the *IM* would be the spectral acceleration at the first mode of the structure,  $Sa(T_1)$ . Offering considerable improvements in terms of *sufficiency* and *efficiency* (Luco and Cornell 2007) the scalar *IM* of *AvgSA* is preferred instead. It is defined by the geometric mean of spectral acceleration over a period range capturing periods both higher and lower than  $T_1$  (Vamvatsikos and Cornell 2005; Kohrangi et al. 2007, 2016a; Eads et al. 2016). In an attempt to capture the higher mode response and period elongation effects of all buildings with the same *IM*, *AvgSA* is computed considering 31 linearly spaced spectral ordinates over a period window of [0.1, 3.1]s, using an increment of 0.1s. The spectral ordinates used to compute *AvgSA* are the geometric mean of the two horizontal components. The lower bound of the period range is set to  $T_2$  of the stiffest structure and an upper bound set at approximately 1.7 times  $T_1$  of the most flexible structure, as indicated in Table 2. Although a building-specific definition of *AvgSA* can be tailored for better fidelity to the specific building and response ductility demand, the single *IM* definition used is not expected to affect the conclusions of this study and has the advantage of allowing for a direct comparison between building fragilities.

PSHA is performed to compute the hazard for *AvgSA* and PGA at the three selected sites of Athens, Perugia and Focsani using OpenQuake (Monelli et al. 2012) considering all seismic sources within 200 km of each site and a  $V_{S30}$  of 360 m/s, consistent with the design assumption. The ESHM13 area source hazard model (Giardini 2013) is used with the Boore and Atkinson ground motion prediction equation (BA08 GMPE) (Boore and Atkinson 2008), employing the indirect method of Kohrangi et al. (2018) to produce the hazard in terms of *AvgSA*. The dashed lines in Figure 5 show the resulting hazard curves for *AvgSA*. Figure 6a compares the 10/50 UHS to the EC8 design spectrum and Figure 6b shows the corresponding pseudo spectral displacement generated from the acceleration spectra assuming that the peak response is governed by the equations of steady-state sinusoidal response. The solid black lines in Figure 6 show the EC8 design spectrum adopted in DDBD, modified by extending the constant velocity region until a corner period of 4.0 seconds. For all sites the PGA level is identical by choice, but all 10/50 spectral ordinates above 0.2s are less severe than the conservative EC8 spectrum, both in terms of acceleration and displacement. Therefore, the performance of each of the six designs at a given site is influenced by two aspects: (i) the effect of inconsistency between the generally conservative assumptions that are behind the shape of the EC8 design spectrum and the hazard at the site (i.e. Figure 6) and, (ii) the effect that the DDBD method has on the building performance. It would not be fair to criticize DDBD for the mismatch between the code and the site hazard; therefore, an additional set of hazard curves are produced for the three sites. To achieve this consistency, the MAR of the individual hazard curves for  $Sa(T_i)$  are uniformly scaled such that the resulting 10/50 UHS approximately matches the design spectrum in the constant-velocity region between 0.6s to 2.0s using the method of least squares. The hazard curves for *AvgSA* are then scaled by this site-specific scale factor. This ensures that there is practically no mismatch between the 10/50 spectral ordinates

and the design spectra at the over the region dominating the response of all structures. The solid lines in Figure 5 and Figure 6a, show the resulting EC8-consistent hazard curves and UHS, respectively. This method of hazard scaling is akin to uniformly increasing the activity rates of all seismic sources that contribute to the hazard, while maintaining the causal distributions of magnitudes and distances that are characteristic of the three sites. Therefore, the relative contributions to the hazard from different earthquake scenarios are identical for both sets of hazard curves, and records selected utilising the disaggregation results are equally representative.

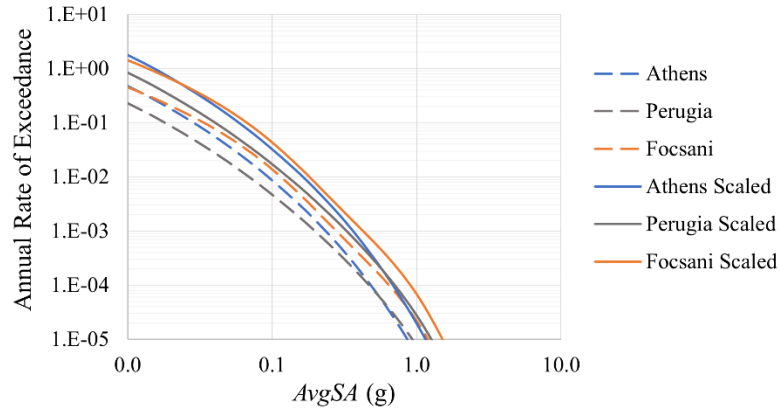


**Figure 5: PSHA results obtained for the three sites in Athens, Perugia and Focsani, showing the seismic hazard curves for AvgSA. Dashed lines indicate the original hazard per site, while the solid lines shows the effect of scaling the UHS to match the design spectrum in the constant velocity region.**

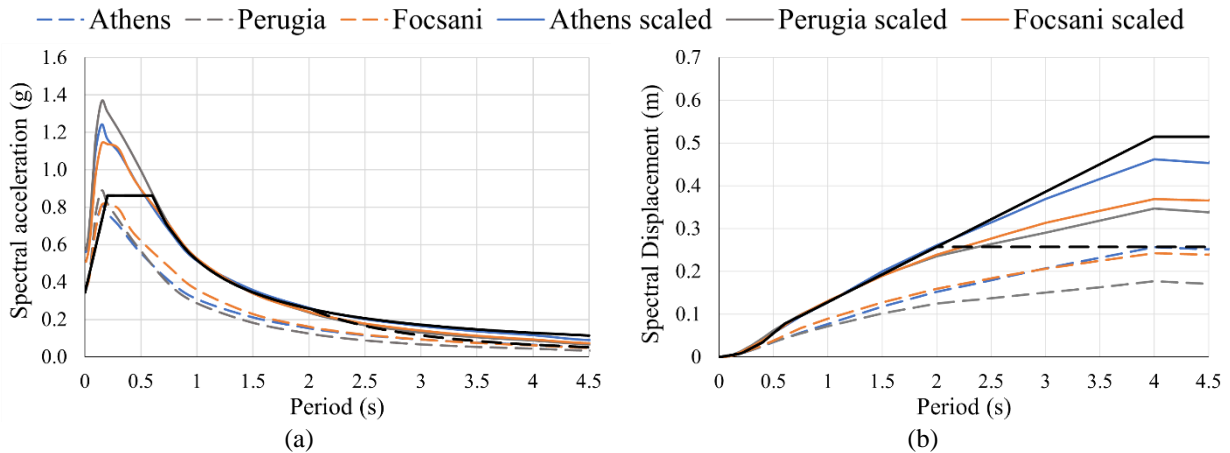


**Figure 6: PSHA results obtained for the three sites in Athens, Perugia and Focsani, showing: (a) site-specific 10/50 UHS and (b) the corresponding pseudo spectral displacement. Both overlaid by the EC8 Type 1 spectrum (dashed black line) and design spectrum adopted in DDBD (solid black line).**

To identify the relative contribution of the causal magnitudes and source to site distances at each intensity level, disaggregation analysis is performed at ten *IM* levels of AvgSA, corresponding to a PoE in 50 years of 70%, 50%, 30%, 10%, 5%, 2%, 1.5%, 1.0%, 0.6% and 0.2%. The corresponding AvgSA values are listed in Table 3, with the mean magnitude and distance that contributes to the hazard level at each site. Figure 7 shows the disaggregation bar charts corresponding to the 10/50 PoE for each site.

**Table 3: The mean magnitude  $\bar{M}$  and distance  $\bar{R}$  resulting from disaggregation at the ten AvgSA IM levels for each of the three selected sites.**

PoE/50 (%)	Return Period (years)	Athens			Perugia			Focsani		
		IM (g)	$\bar{M}$ ( $M_w$ )	$\bar{R}$ (km)	IM (g)	$\bar{M}$ ( $M_w$ )	$\bar{R}$ (km)	IM (g)	$\bar{M}$ ( $M_w$ )	$\bar{R}$ (km)
70	42	0.06	6.7	53	0.04	6.1	33	0.08	6.5	25
50	72	0.08	6.8	44	0.06	6.2	26	0.10	6.6	21
30	140	0.11	6.9	34	0.08	6.3	20	0.13	6.8	17
10	475	0.18	7.0	20	0.14	6.4	12	0.21	6.9	12
5	975	0.23	7.1	16	0.2	6.5	10	0.27	7.0	10
2	2475	0.32	7.2	12	0.28	6.6	8	0.39	7.1	9
1.5	3308	0.35	7.2	11	0.31	6.7	8	0.43	7.2	8
1.0	4975	0.39	7.3	10	0.37	6.7	8	0.50	7.2	8
0.6	8308	0.46	7.3	9	0.44	6.8	8	0.60	7.2	8
0.2	24975	0.62	7.4	8	0.63	6.8	8	0.84	7.3	8

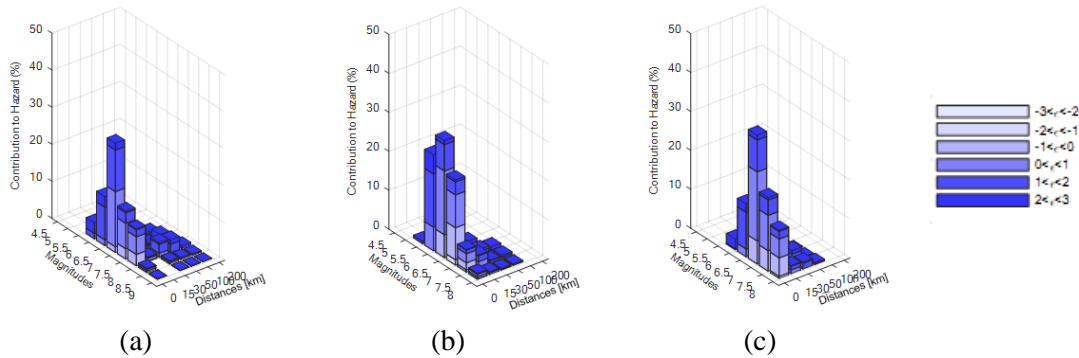


**Figure 7: Disaggregation results for selected sites located in (a) Athens; (b) Perugia; and, (c) Focsani, conditioned on the 10/50 AvgSA level.**

Structural response may depend on characteristics of the seismic hazard at the site where the structure is located that go beyond the selected IM (Kohrangi et al. 2017). Record selection provides the missing link. The robustness of this link, and ultimately the reliability of the results, is largely dependent on how well the characteristics of the hazard are represented by the chosen ground motion set and the quality of the chosen IM. As shown in Figure 7, the distribution of the causal magnitudes and source to site distances vary between the three sites at the same intensity level. When extending this comparison to all intensity levels, the causal parameters can vary considerably. It is therefore desired to select a record set for each intensity level, unique to each site, which reflects these changes in the ground motion characteristics. To maintain hazard consistency in the evaluation of the seismic risk, the conditional spectra (CS) (Kohrangi et al. 2007; Lin et al. 2013b) based record selection approach is adopted, where hazard consistency is maintained with respect to the intensity dependent spectral shape. For each site, 20 two-component ground motions are selected from the PEER NGA database (Gokkaya et al. 2016) for each of the ten AvgSA levels listed in Table 3. The selected ground motions are scaled to collectively match the target mean and variance of the geometric mean spectral acceleration of the two horizontal components, using the algorithm of Kohrangi (2015). In the generation of the CS target, we used the BA08 GMPE and the period-to-period spectral acceleration correlation model of Baker and Jayaram (2008). The selection is performed based on the *exact* method in which all the causal events in the disaggregation analysis are considered in generating the CS target spectrum (Lin et al. 2013a). Figure 8 shows the excellent matching achieved between the statistics extracted from the selected record sets compared to the AvgSA-based CS defined target.

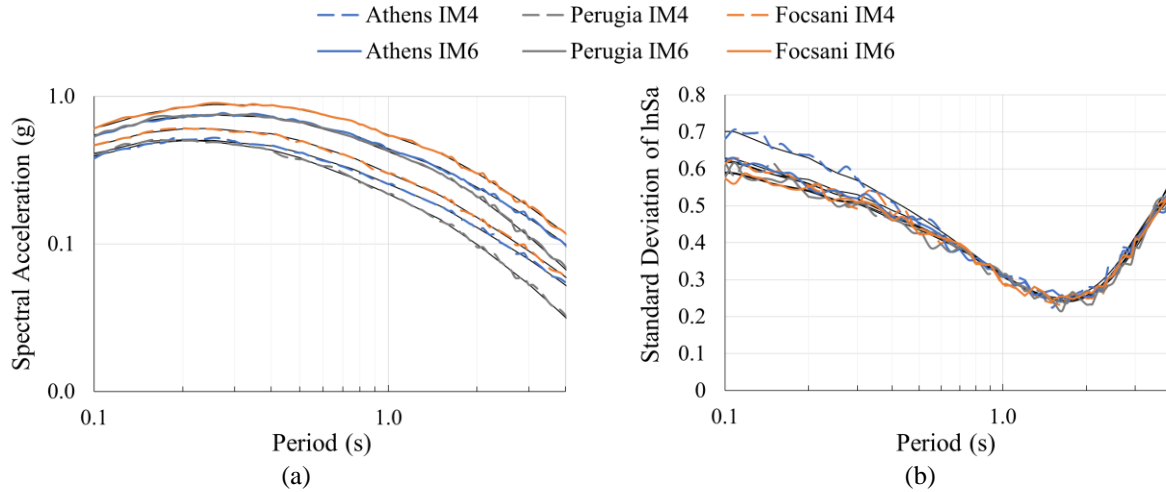


**Figure 8: (a) Median and (b) standard deviation of  $\ln(S_a)$  for the selected record sets at the three sites compared to the CS target (black lines) conditioned on the 10/50 and 2/50 *IM* levels with corresponding return periods of 475 years (IM4), and 2475 years (IM6).**

## STRUCTURAL RESPONSE AND BUILDING PERFORMANCE

For each of the 18 building-site variants, MSA is performed using the 20 selected ground motions at each of the 10 *IM* levels. As 2D models are employed, they are subjected to only one horizontal component per pair, chosen at random. Figure 9 shows the MIDR results for the 4-storey wall-steel frame and the 9-storey RC wall buildings located at the three sites. Despite MSA being performed with stripes up to an intensity level with a return period of 25,000 years, the hazard is not severe enough to produce meaningful collapse data for the 4-storey dual building located in Perugia, as shown in Figure 9a. This is the only building variant with limited collapse data and the effect of this is reflected by the very low GC rate in its MIDR hazard curve. Given that the probability of exceeding the highest intensity level is 0.2% in 50 years, i.e., extremely rare, supplementing the existing data with additional stripes capable of causing collapse will have a negligible influence on the estimated GC risk.

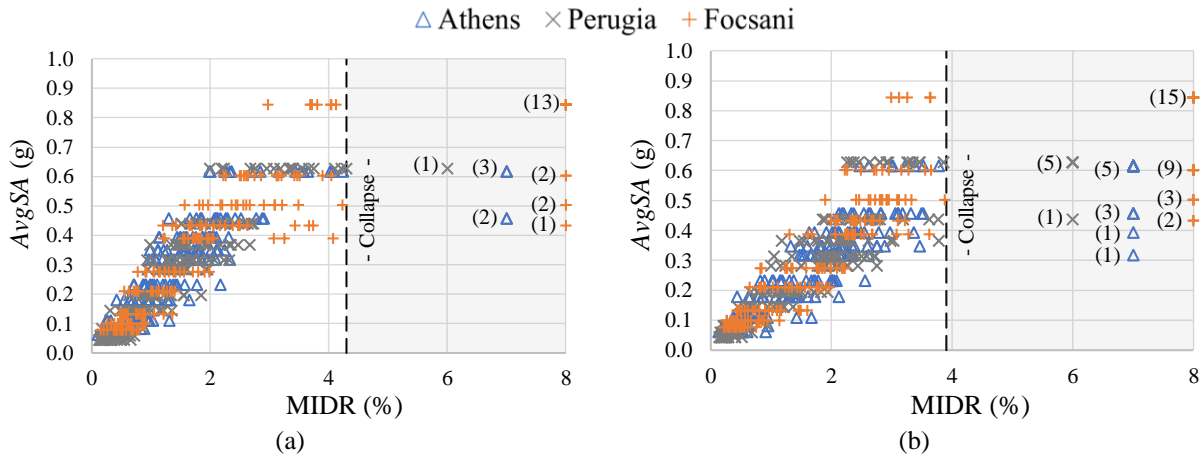


**Figure 9: MSA results of (a) the 4-storey wall-steel frame building and (b) 9-storey wall building located in Athens, Perugia and Focsani. Results that indicate collapse, are lumped at an MIDR value past the collapse capacity (dashed line), with the number of records causing collapse in that stripe indicated in parentheses.**

Lognormal fragility functions are fitted for the 18 building-site variants using the maximum likelihood method (Baker 2015). Figure 10 shows the fragility curves in terms of the probability of the MIDR exceeding the LS limit state (i.e.,  $MIDR > 2\%$ ) and for GC. Additional uncertainty, e.g., due to the imperfect knowledge in structural

modelling parameters, is taken to offer an additional dispersion of 0.25. This is incorporated by adopting the common first-order assumption, whereby the median response remains the same and the dispersion is augmented by the additional uncertainty in a square-root-of-the-sum-of-squares fashion. Figure 10a compares the fragility curves of the 4-storey wall building located in Focsani with and without considering the structural modelling variability; it shows that in the presence of additional sources of uncertainty, the probability of exceeding the limit state capacity increases for intensities less than the median capacity but decreases for intensities higher than the median. As a consequence, ground motions with a lower intensity but higher rate of occurrence are capable of contributing more to the risk of exceeding the limit state capacity.

By comparing the fragility functions shown in Figure 10b, not surprisingly, it can be seen that the limit state median capacity of these DDBD buildings in terms of the ground motion intensity is both building-dependent and, more importantly, site-dependent. More specifically, as also found in Kohrangi et al. (2017b), identical buildings located at different sites do not have the same median LS and GC capacities. For instance, the estimates of the median GC capacity of the 9-storey dual system buildings are  $AvgSA = 0.57g$ ,  $0.73g$  and  $0.63g$  when located in Athens, Perugia and Focsani, respectively. This difference is due to the different spectral characteristics of the ground motions that may occur at the three different sites, despite the 10/50 PGA, and the design response spectrum being identical.

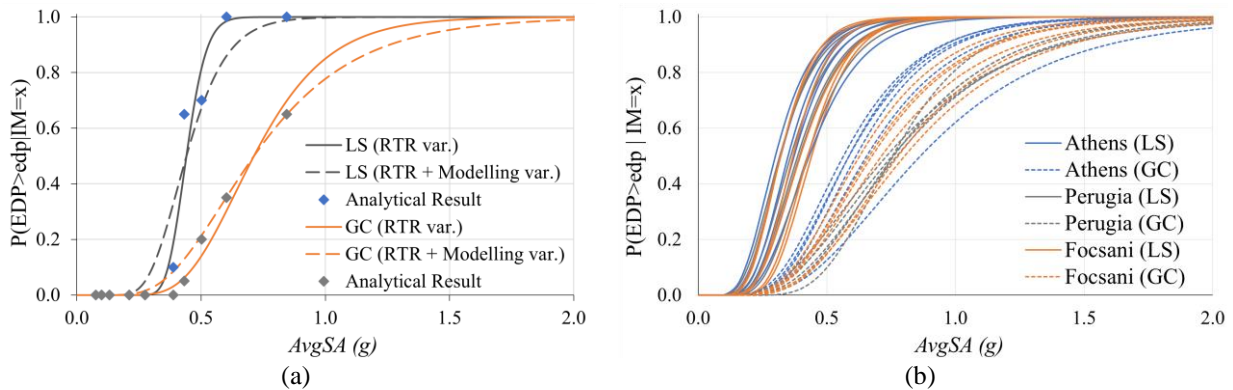


**Figure 10: Fragility functions for LS (MIDR>2.0%) and GC limit state showing: (a) effect of record-to-record variability (RTR var) with and without modelling uncertainty for the 4-storey wall building located in Focsani; and (b) fragility functions of all 18 building-site variants accounting for both types of uncertainty.**

Similar to the characterisation of the LS and GC exceedance shown in Figure 10b, the MSA results are used to produce additional fragility curves to characterize the exceedance of MIDR levels from 0.1% to 10%. The full set of fragility curves are convolved with the two sets of unscaled and scaled hazard curves (Figure 5a) using the reduced version of Equation (1) to characterise the MAR of exceeding this wide range of MIDR values (i.e.,  $\lambda(EDP)$  in the format of Equation 1). The outcome is represented in the form of MIDR hazard curves. The results of the unscaled hazard curves in Figure 11a show the full effect seen by a practitioner using DDBD with the EC8 design spectrum with a return period of 475 years. For these buildings the MAR of exceeding DL (i.e., MIDR > 1%) varies from  $1.7 \times 10^{-3}$  to  $7.1 \times 10^{-3}$ , while for LS (MIDR > 2%) the range is from  $2.4 \times 10^{-4}$  to  $1.5 \times 10^{-3}$ . The equivalent return periods vary between 140 to 590 years and 670 to 4170 years for the DL and LS limit states, respectively. The MAR of GC is also far from being uniform: it varies by an order of magnitude from approximately  $10^{-4}$  to  $10^{-5}$ , corresponding to a return period range between 10,000 and 100,000 years. At the same time, and more interestingly for the discussion here, Figure 11b reveals the wide variation in the building performance due only to the application of to the DDBD method itself, using the scaled EC8 consistent hazard curves. Again, the MAR values of exceeding the three limit states vary greatly across sites and across buildings, a result that confirms the non-uniformity of the performance of buildings designed via DDBD.

More specifically, how do these MAR values of MIDR limit state thresholds obtained using both sets of hazard curves (Figure 10a and b) translate into PoEs in 50 years? Here we recall that the DDBD method targeted only the LS limit state of the buildings by imposing a drift limit of 2.0% at a design ground motion intensity level with a 10/50 PoE. Thus, the designer may be led to believe that buildings designed based on this approach should have a PoE for LS equal to, or less than 10/50, that is, the same value associated with the design spectrum. Making the common assumption of PSHA that the Poisson distribution can adequately represent the occurrence in time of earthquake events, we first compute the PoE in 50 years of the design performance objective of LS shown in Figure 12. Results

from original versus EC8-compatible hazard are indicated by the solid and hatched bars, respectively. Similarly, Figure 13a and Figure 13b show the PoE in 10 years for DL and the PoE in 50 years for GC, respectively.

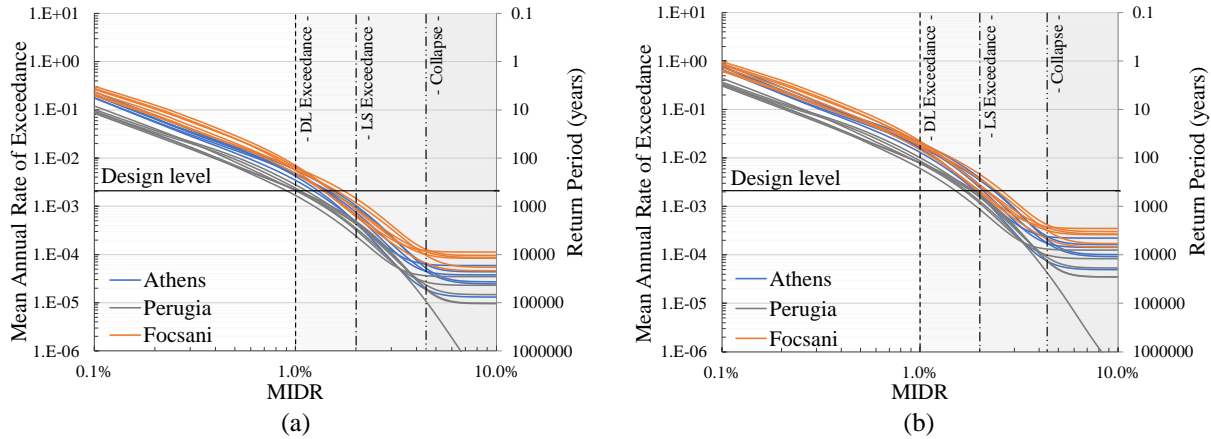


**Figure 11: MIDR hazard curves obtained using: (a) the site hazard curves; and (b) the “EC8 consistent” scaled hazard curves.**

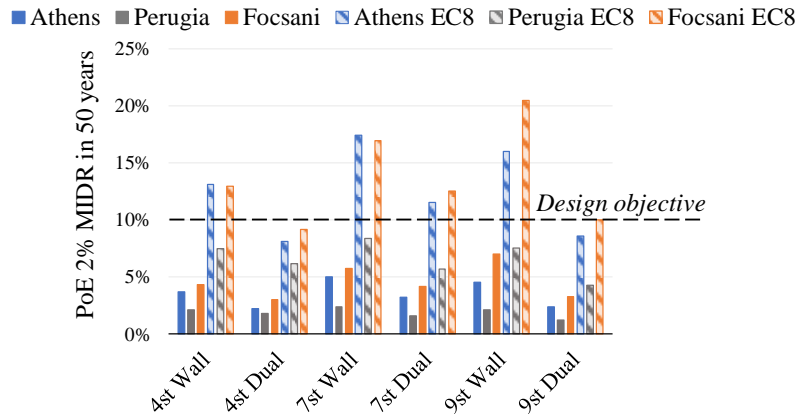


**Figure 12: LS performance obtained using the site hazard (solid bars) and the “EC8 consistent” scaled hazard (hatched bars).**

As stated earlier, the first obvious observation from the results presented in Figure 12 is that checking the PoE of the design intensity is not equivalent to checking the PoE of the limit state performance targeted in the design procedure. With reference to the solid bars in Figure 12, the PoE of the target MIDR limit is in the range of 1.2%–7.0% in 50 years, and is on average 67% lower than the PoE of the 10/50 design ground motion intensity. This implies that these buildings conservatively conform to the code requirements and thus, they satisfy the pre-defined performance objective. This conservatism, however, is clearly imposed by the effect of the overly severe demand dictated by the EC8 Type 1 design spectrum (see black lines in Figure 6). Pick a different site of the same 10/50 PGA where the code spectrum happens to be unconservative and the conclusion may well be reversed. A fairer evaluation of the DDBD approach, however, can be made from the comparison of the hatched bars in Figure 12 obtained using the scaled, EC8-consistent hazard curves. This better reveals the effectiveness of DDBD in achieving the performance objective targeted in the design. With this modification, the average LS PoE increases to 11.0% in 50 years, ranging from 4.2% to 20.5% in 50 years. Although, on average, the LS is marginally satisfied (i.e., PoE 11/50 versus the target of 10/50) for the ensemble of building-site variants evaluated, the results differ from case to case: LS is not satisfied for 8 out of 12 buildings in Athens and Focsani, while all 6 buildings located in Perugia are deemed LS-compliant by a good margin. In plain words, DDBD does not necessarily satisfy its target design objective, but also it does not

guarantee a uniform risk of the performance objectives not being met. FBD is no stranger to this problem as well, owing to its intensity rather than risk basis.

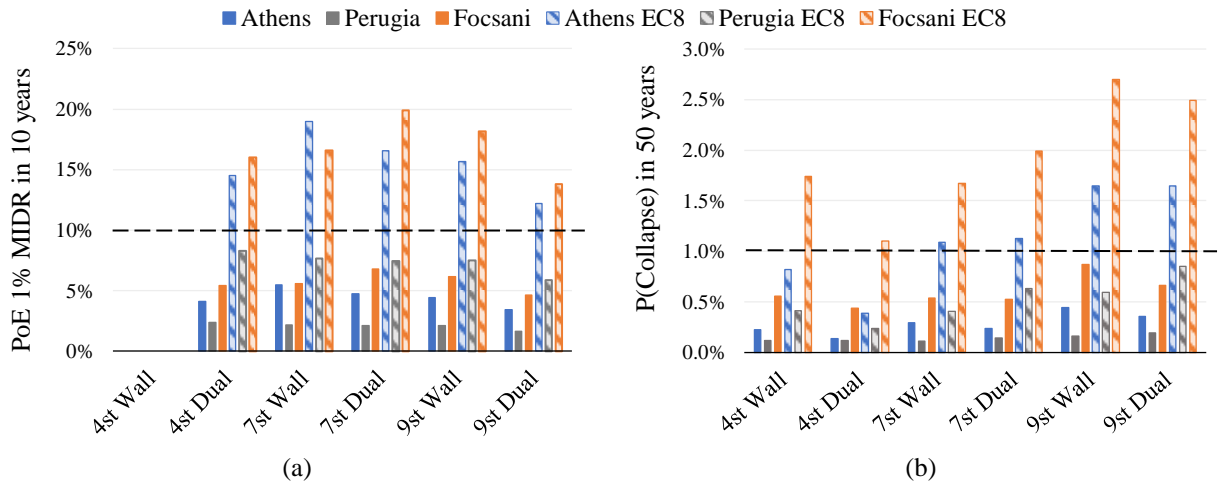


**Figure 13: Limit state performance for (a) DL criteria and, (b) GC criteria; corresponding to the site hazard (solid bars) and the “EC8 consistent” scaled hazard (hatched bars).**

As previously mentioned, the building designs for 15 of the 18 building-site variants are governed by the LS limit state and therefore, according to the DDBD procedure, these buildings automatically satisfy the DL requirement of EC8. That is, the DDBD procedure implies that the DL drift limit of 1.0% is achieved for an intensity level corresponding to a PoE lower than 10/10. However, despite being designed for a base shear larger than that required to satisfy the DL requirement, the probability of exceeding the DL criterion (see Figure 13a) is on average 13% in 10 years, with a wide range in the performance of 0.6 (for the 9-storey dual building in Athens) to 2.0 times (for the 7-storey dual building in Focsani) the 10% PoE assigned to the DL design spectrum. In fact, as seen by the MIDR hazard curves in Figure 11, large differences in the MAR are observed at all MIDR levels.

Figure 13b similarly shows the PoE of GC in 50 years. Unlike the previous limit states, extending the performance evaluation to the GC limit state is not a straight forward task as no clear consensus on the tolerable collapse risk exists. As shown by Spillatura (2018) attempts in the previous literature have been made to target GC performance using risk-targeted spectra; however, the “acceptable” target GC risk in these studies varied considerably and with no robust justification. Previous versions of the international building code (IBC) and ASCE/SEI 7-10 (IBC 2012; ASCE 2013) stipulated ordinary buildings to have a risk-targeted “acceptable” GC PoE of 1/50 or, equivalently, a MAR of collapse equal to, or less than,  $2.0 \times 10^{-4}$ . However, the pertaining requirements in these documents have been removed in the subsequent versions. More recently, Tsang and Wenzel (2016) evaluated the previous collapse risk requirements of IBC by linking the GC rate to the expected mortality rate using a tolerable annual mortality rate of  $10^{-6}$ ; the same order of magnitude accepted for other natural catastrophes. The study determined that a target MAR of GC less than  $2.0 \times 10^{-4}$  is adequate for controlling fatality risk of less vulnerable buildings such as lightweight steel and timber construction, but a uniform target for all buildings of less than  $1.0 \times 10^{-4}$  is recommended. Herein, an “acceptable” GC PoE of 1/50 has been adopted as the target to evaluate the GC performance of the buildings designed via DDBD.

Regarding the EC8-consistent results displayed in Figure 13b, the average GC PoE of the case study buildings is 1.2% in 50 years, only 20% higher than the somewhat arbitrary target of 1.0%. However, what matters the most here is the significant difference in the degree of safety, with collapse risk estimates varying by more than a factor of 10 (from 0.2% to 2.7% in 50 years) across the 18 buildings considered. Furthermore, it is worthwhile noting that by comparing Figure 12 to Figure 13b, it is clear that targeting only LS performance—as done in DDBD and most applications of FBD—cannot guarantee collapse performance without considering the site-specific hazard characteristics. For example, as shown in Figure 5, the sites in Athens and Focsani have similar (scaled) hazard curves at the levels most contributing to the exceedance of the LS limit state (i.e., from  $5 \times 10^{-2}$  to  $1 \times 10^{-3}$ ) with the hazard curves deviating at intensities that control the GC risk (i.e., above  $1 \times 10^{-3}$ ). As a consequence, the four-storey wall building in Athens and Focsani have essentially the same risk of exceeding the LS objective (i.e., PoE of 13/50, see

Figure 12), but with a difference in the collapse risk of more than double (0.8/50 in Athens versus 1.7/50 in Focsani, see Figure 13b). These results clearly indicate that DDBD lacks the ability to control or target the GC performance by designing to the LS performance level; in other words, the verification of the LS performance reveals little about GC performance. To be fair, the same issues plague FBD as demonstrated by Iervolino et al. (2019), owing to the intensity basis of both methods.

The highly non-uniform risk obtained in this study highlights, once more, why the degree of confidence in having achieved the performance objective should be questioned when neglecting hazard characteristics other than that at the design intensity, as well as sources of uncertainty inherent in the IM–EDP relationship. As shown by O’Reilly and Calvi (2020), when these aspects are accounted for even in an approximate manner using closed-form solutions in tandem with DDBD, significant improvements in the reliability of the response can be achieved.

## CONCLUSIONS

The seismic design of structures involves designing a single system to achieve several “acceptable” performance objectives subject to the demand imposed by a highly complex phenomenon. As such, practitioners depend on the capabilities of design procedures to provide reliable estimates of the building performance and safety to facilitate meaningful design decisions and the communication of risk to the relevant stakeholders. The current state-of-the-art procedure of probabilistic performance-based earthquake engineering (PBEE) is arguably the most reliable framework for mapping the seismic hazard to the structural response and can provide benchmark estimates of the seismic performance of a building. However, the sophistication and complexity of such a method puts it out of reach for the design of the majority of structures built in today’s society. If one is to adopt a simplified alternative, as is done routinely, it should be made clear what is being traded for practicality. This study investigated the ability of the innovative design philosophy known as Direct Displacement-Based Design (DDBD) to (i) approach the more robust response estimates that can be achieved with the advanced PBEE methods, and to (ii) provide insight into the capabilities of DDBD to alleviate the computational burden. A state-of-the-art application of probability theory is used to fully characterise the risk of exceeding maximum inter-storey drift ratio thresholds associated with three limit states for six buildings, each located at three high-seismicity European sites, by employing the PEER PBEE methodology. Hence, this exercise explored 18 building-site variants. The exact conditional spectrum method based on the intensity measure of  $AvgSA$  is used to select 200 ground motions for each site to link the seismic hazard to the structural response at ten discrete intensity levels. The outcome of this process indicates that DDBD, on average, resulted in a building performance close to the initial performance objective, but also uncovered a considerable variation in the performance achieved. Almost 50% of the building-site variants were found to fail the initial performance objective targeted by the DDBD method (i.e., Life Safety at the 10% in 50 years design level) and to have a significant difference in the degree of safety achieved, with collapse rates varying by more than a factor of 10. This exercise demonstrates, once again, the trade-off of a practical design method that is capable of achieving the performance objective approximately but not for all sites or building types. The application of DDBD produces code conforming structures with a highly non-uniform risk. If one is to achieve the design objectives of a specific structure with a meaningful degree of confidence, DDBD cannot replace the computationally demanding probabilistic methods embraced by PBEE unless enhancements are implemented.

## ACKNOWLEDGEMENTS

The first author acknowledges the support and funding from The University School for Advanced Studies IUSS Pavia. Financial support has also been provided by the European Commission through the Horizon 2020 programs "HYPERION–Development of a decision support system for improved resilience & sustainable reconstruction of historic areas to cope with climate change & extreme events based on novel sensors and modelling tools", Grant Agreement No. 821054, and "YADES - Improved Resilience and Sustainable Reconstruction of Cultural Heritage Areas to cope with Climate Change and Other Hazards based on Innovative Algorithms and Modelling Tools", Grant Agreement No. 872931.

## REFERENCES

- Ancheta, T.D., Darragh, R.B., Stewart, J.P., Seyhan, E., Silva, W.J., Chiou, B.S.J., Wooddell, K.E., Graves, R.W., Kottke, A.R., Boore, D.M. and Kishida, T., 2014. NGA-West2 database. *Earthquake Spectra*, 30(3), pp.989-1005.
- ASCE/SEI (2017) Minimum Design Loads and Associated Criteria for Buildings and Other Structures. American Society of Civil Engineers, Reston, VA
- ASCE (2013) Minimum Design Loads for Buildings and Other Structures, ASCE/SEI 7-10. American Society of Civil Engineers, Reston, VA
- Baker JW (2015) Efficient Analytical Fragility Function Fitting Using Dynamic Structural Analysis. *Earthq Spectra* 31:579–599. <https://doi.org/10.1193/021113EQS025M>
- Baker JW, Jayaram N (2008) Correlation of Spectral Acceleration Values from NGA Ground Motion Models. *Earthq Spectra* 24:299–317. <https://doi.org/10.1193/1.2857544>
- Bazzurro P, Cornell CA, Shome N, Carballo JE (1998) Three Proposals for Characterizing MDOF Nonlinear Seismic Response. *J Struct Eng* 124:1281–1289. [https://doi.org/10.1061/\(asce\)0733-9445\(1998\)124:11\(1281\)](https://doi.org/10.1061/(asce)0733-9445(1998)124:11(1281))
- Boore DM, Atkinson GM (2008) Ground-motion prediction equations for the average horizontal component of PGA, PGV, and 5%-damped PSA at spectral periods between 0.01 s and 10.0 s. *Earthq Spectra* 24:99–138. <https://doi.org/10.1193/1.2830434>
- CEN (2004a) Design of structures for earthquake resistance - Part 1 : General rules, seismic actions and rules for buildings, (EN1998-1:2004). Brussels: Comité Européen de Normalization
- CEN (2004b) Design of concrete structures -Part 1: General rules and rules for buildings, (EN1992 -1-1: 2004). Brussels: Comité Européen de Normalization. European Committee for Standardization
- CEN (2005) Design of steel structures - Part 1-1: General rules and rules for buildings (EN1993-1-1:2005). Brussels: Comité Européen de Normalization
- Cornell CA (1968) Engineering seismic risk analysis. *Bull Seismol Soc Am* 1583–1606. [https://doi.org/http://dx.doi.org/10.1016/0167-6105\(83\)90143-5](https://doi.org/http://dx.doi.org/10.1016/0167-6105(83)90143-5)
- Cornell CA, Jalayer FJ, Hamburger RO, Foutch DA (2002) Probabilistic Basis for 2000 SAC Federal Emergency Management Agency Steel Moment Frame Guidelines. *J Struct Eng*. [https://doi.org/10.1061/\(ASCE\)0733-9445\(2002\)128](https://doi.org/10.1061/(ASCE)0733-9445(2002)128)
- Cornell CA, Krawinkler H (2000) Progress and Challenges in Seismic Performance Assessment. *PEER Cent News*
- Deierlein GG, Krawinkler H, Cornell CA (2003) A framework for performance-based earthquake engineering. *Proc 2003 Pacific Conf Earthq Eng* 273:140–148. <https://doi.org/10.1061/9780784412121.173>
- Eads L, Miranda E, Lignos D (2016) Spectral shape metrics and structural collapse potential. *Earthq Eng Struct Dyn* 45:1643–1659. <https://doi.org/10.1002/eqe.2739>
- Faccioli E, Paolucci R, Rey J (2004) Displacement spectra for long periods. *Earthq Spectra* 20:347–376. <https://doi.org/10.1193/1.1707022>
- FEMA (2018) Seismic Performance Assessment of Buildings. Volume 1 – Methodology. Fema P-58
- FEMA (2009) Quantification of building seismic performance factors
- Franchin P, Petrini F, Mollaioli F (2018) Improved risk-targeted performance-based seismic design of reinforced concrete frame structures. *Earthq Eng Struct Dyn*. <https://doi.org/10.1002/eqe.2936>
- Franchin P, Pinto PE (2012) Method for Probabilistic Displacement-Based Design of RC Structures. *J Struct Eng*. [https://doi.org/10.1061/\(asce\)st.1943-541x.0000492](https://doi.org/10.1061/(asce)st.1943-541x.0000492)
- Garcia R, Sullivan TJ, Corte G Della (2010) Development of a displacement-based design method for steel frame-RC wall buildings. *J Earthq Eng* 14:252–277. <https://doi.org/10.1080/13632460902995138>
- Giardini D et al. (2013) Seismic Hazard Harmonization in Europe (SHARE). In: Online data Resour. Swiss Seismol.

- Serv. ETH Zurich, Zurich, Switz. <http://www.efehr.org:8080/jetspeed/>
- Giardini D, Wössner J, Danciu L (2014) Mapping Europe's seismic hazard. *Eos* (Washington DC). <https://doi.org/10.1002/2014EO290001>
- Gokkaya BU, Baker JW, Deierlein GG (2016) Quantifying the impacts of modeling uncertainties on the seismic drift demands and collapse risk of buildings with implications on seismic design checks. *Earthq Eng Struct Dyn* 45:1661–1683. <https://doi.org/10.1002/eqe.2740>
- IBC (2012) ICC, 2012. International Building Code (IBC).
- Iervolino I, Spillatura A, Bazzurro P (2018) Seismic Reliability of Code-Conforming Italian Buildings. *J Earthq Eng*. <https://doi.org/10.1080/13632469.2018.1540372>
- Iervolino I, Spillatura A, Bazzurro P (2019) RINTC-E project: Towards the assessment of the seismic risk of existing buildings in Italy. *COMPdyn Proc* 3:5061–5072. <https://doi.org/10.7712/120119.7288.20038>
- Jalayer F (2003) Direct Probabilistic Seismic Analysis: Implementing Non-Linear Dynamic Assessments. Stanford University: Stanford, CA
- Kohrangi M (2015) CS(AvgSA) Matlab routines to estimate the Conditional Spectrum conditioned on given values of the average spectral acceleration, AvgSa, and to select hazard-consistent records to match it. Accessible at: <http://users.ntua.gr/divamva/software.html>
- Kohrangi M, Bazzurro P, Vamvatsikos D (2016a) Vector and Scalar IMs in Structural Response Estimation, Part II: Building Demand Assessment. *Earthq Spectra* 32:1525–1543. <https://doi.org/10.1193/053115EQS081M>
- Kohrangi M, Bazzurro P, Vamvatsikos D, Spillatura A (2007) Conditional spectrum-based ground motion record selection using average spectral acceleration. *Earthq Eng Struct Dyn* 46:1667–1685. <https://doi.org/10.1002/eqe.2876>
- Kohrangi M, Kotha SR, Bazzurro P (2018) Ground-motion models for average spectral acceleration in a period range: direct and indirect methods. *Bull Earthq Eng* 16:45–65. <https://doi.org/10.1007/s10518-017-0216-5>
- Kohrangi M, Vamvatsikos D, Bazzurro P (2016b) Implications of Intensity Measure Selection for Seismic Loss Assessment of 3-D Buildings. *Earthq Spectra* 32:2167–2189. <https://doi.org/10.1193/112215EQS177M>
- Kohrangi M, Vamvatsikos D, Bazzurro P (2017) Site dependence and record selection schemes for building fragility and regional loss assessment. *Earthq Eng Struct Dyn* 46:1625–1643. <https://doi.org/10.1002/eqe.2873>
- Krawinkler H, Zareian F, Medina RA, Ibarra LF (2006) Decision support for conceptual performance-based design. *Earthq Eng Struct Dyn* 35:115–133. <https://doi.org/10.1002/eqe.536>
- Lignos DG, Krawinkler H (2011) Deterioration Modeling of Steel Components in Support of Collapse Prediction of Steel Moment Frames under Earthquake Loading. *J Struct Eng*. [https://doi.org/10.1061/\(asce\)st.1943-541x.0000376](https://doi.org/10.1061/(asce)st.1943-541x.0000376)
- Lin T, Harmsen SC, Baker JW, Luco N (2013a) Conditional spectrum computation incorporating multiple causal earthquakes and ground-motion prediction models. *Bull Seismol Soc Am* 103:1103–1116. <https://doi.org/10.1785/0120110293>
- Lin T, Haselton CB, Baker JW (2013b) Conditional spectrum-based ground motion selection. Part I: Hazard consistency for risk-based assessments. *Earthq Eng Struct Dyn* 42:1847–1865. <https://doi.org/10.1002/eqe.2301>
- Luco N, Cornell CA (2007) Structure-Specific Scalar Intensity Measures for Near-Source and Ordinary Earthquake Ground Motions. *Earthq Spectra* 23:357–392. <https://doi.org/10.1193/1.2723158>
- Luco N, Ellingwood BR, Hamburger RO, et al (2007) Risk-targeted versus current seismic design maps for the conterminous united states. In: Structural Engineering Association of California 2007 Convention Proceedings
- Mander JB, Priestley MJN, Park R (1988) Theoretical stress-strain model for confined concrete. *Journal of Structural Engineering*, Vol. 114, No. 8, pp. 1804–1826.
- Menegotto M, Pinto PE (1973) Method of analysis for cyclically loaded R.C. plane frames including changes in geometry and non-elastic behaviour of elements under combined normal force and bending. *Int Assoc Bridg*

- Moehle JP (1992) Displacement-Based Design of RC Structures Subjected to Earthquakes. *Earthq. Spectra* 8:403–428
- Monelli D, Pagani M, Weatherill G, et al (2012) The hazard component of OpenQuake: The calculation engine of the Global Earthquake Model. 15th World Conf Earthq Eng
- NZS (2004) Structural Design Actions - Part 5: Earthquake actions- New Zealand, (NZS 1170.5:2004). New Zealand Standards (NZS)
- O'Reilly GJ, Calvi GM (2020) Quantifying seismic risk in structures via simplified demand–intensity models. *Bull Earthq Eng* 18:2003–2022. <https://doi.org/10.1007/s10518-019-00776-0>
- O'Reilly GJ, Calvi GM (2019) Conceptual seismic design in performance-based earthquake engineering. *Earthq Eng Struct Dyn* 48:389–411. <https://doi.org/10.1002/eqe.3141>
- Porter KA, Beck JL, Shaikhutdinov R V. (2002) Sensitivity of building loss estimates to major uncertain variables. *Earthq Spectra* 18:719–743. <https://doi.org/10.1193/1.1516201>
- Priestley MJ., Calvi G., Kowalsky MJ (2007) *Displacement-Based Seismic Design of Structures*, 1<sup>st</sup> edn. Fondazione Eucentre, Pavia, Italy
- Priestley NMJ (1993) Myths and fallacies in earthquake engineering-conflicts between design and reality. *Bull New Zeal Natl Soc Earthq Eng*
- SeismoSoft (2018) *SeismoStruct* (2018): A computer program for static and dynamic nonlinear analysis of framed structures. Available from URL <https://seismosoft.com/>
- Shahnazaryan D, O'Reilly GJ (2021) Integrating expected loss and collapse risk in performance-based seismic design of structures. *Bull Earthq Eng*. <https://doi.org/10.1007/s10518-020-01003-x>
- Shibata A. and Sozen M., (1976) Substitute structure method for seismic design in reinforced concrete. *ASCE Journal of Structural Engineering*, Vol 102(1), pp 1-18
- Spillatura A (2018) *From Record Selection to Risk Targeted Spectra for Risk-based Assessment and Design*. Istituto Universitario degli Studi Superiori (IUSS), Pavia
- Spillatura A, Vamvatsikos D, Bazzurro P, Kohrangi M (2019) Issues in harmonization of seismic performance via risk targeted spectra. In: 13th International Conference on Applications of Statistics and Probability in Civil Engineering, ICASP 2019
- Sullivan TJ., Priestley MJN, Calvi GM (2012) *A Model Code for the Displacement-Based Seismic Design of Structures*, DBD12. IUSS Press, Pavia, Italy
- Tsang HH, Wenzel F (2016) Setting structural safety requirement for controlling earthquake mortality risk. *Saf Sci* 86:174–183. <https://doi.org/10.1016/j.ssci.2016.02.028>
- Vamvatsikos D (2017) *Performance-Based Seismic Design In Real Life : The Good, The Bad And The Ugly*. Pisa Univ Press 17–21
- Vamvatsikos D, Aschheim MA (2016) Performance-based seismic design via yield frequency spectra. *Earthq Eng Struct Dyn* 45:1759–1778. <https://doi.org/10.1002/eqe.2727>
- Vamvatsikos D, Bakalis K, Kohrangi M, et al (2020) A risk-consistent approach to determine EN1998 behaviour factors for lateral load resisting systems. *Soil Dyn Earthq Eng* 131:. <https://doi.org/10.1016/j.soildyn.2019.106008>
- Vamvatsikos D, Cornell A (2002) Incremental dynamic analysis. *Earthq Eng Struct Dyn* 31:491–514. <https://doi.org/10.1002/eqe.141>
- Vamvatsikos D, Cornell CA (2005) Developing efficient scalar and vector intensity measures for IDA capacity estimation by incorporating elastic spectral shape information. *Earthq Eng Struct Dyn* 34:1573–1600. <https://doi.org/10.1002/eqe.496>
- Vamvatsikos D, Kazantzi AK, Aschheim MA (2016) *Performance-based seismic design: Avant-garde and code-*

compatible approaches. *ASCE-ASME J Risk Uncertain Eng Syst Part A Civ Eng* 2:1–9. <https://doi.org/10.1061/AJRUA6.0000853>

Wen YK (2001) Reliability and performance-based design. *Struct Saf* 23:407–428. [https://doi.org/10.1016/S0167-4730\(02\)00011-5](https://doi.org/10.1016/S0167-4730(02)00011-5)

Zareian F, Krawinkler H (2012) Conceptual performance-based seismic design using building-level and story-level decision support system. *Earthq Eng Struct Dyn* 41:1439–1453. <https://doi.org/10.1002/eqe.2218>

Žižmond J, Dolšek M (2019) Formulation of risk-targeted seismic action for the force-based seismic design of structures. *Earthq Eng Struct Dyn*. <https://doi.org/10.1002/eqe.3206>